OPTIMIZATION OF THE GAIN MEDIUM DELIVERY SYSTEM FOR AN X-RAY LASER OSCILLATOR *

M. Yadav [†], P. Manwani, B. Naranjo, N. Majernik, J. Rosenzweig
University of California, Los Angeles, USA
A. Halavanau, E. Galtier, C. Pellegrini
SLAC National Accelerator Laboratory, Stanford University, Menlo Park, USA
A. Malinouski, Luikov Heat and Mass Transfer Institute, Minsk, Belarus

Abstract

An X-ray laser oscillator, called XLO, is a recently started project at SLAC to build the first population inversion X-ray laser. XLO utilizes a train of XFEL SASE pulses to pump atomic core-states. The resulting amplified spontaneous emission radiation is recirculated in a back scattering Bragg cavity and subsequently amplified. XLO will provide fully coherent, transform-limited X-ray pulses with 50 meV bandwidth and 1e10 photons. Currently, XLO is being considered for operation at the copper K-alpha line at 8048 eV. In this work, we focus on the optimization of gain medium delivery in the XLO cavity. We consider a fast, subsonic jet of copper nitrate solution, moving through a cylindrical nozzle. We focus on the nozzle geometry optimization and possible diagnostics of the jet-XFEL interaction point. We also discuss the use of a solid state copper medium.

INTRODUCTION

X-ray free electron lasers (XFELs) are a revolutionary tool to explore matter at atomic length and time scales, with femtosecond long pulses of angstrom wavelength. Recently it has been demonstrated XFELs can create population inversion at different inner atomic levels [1–4] and generate amplified spontaneous emission radiation (ASE). XFELs operate in SASE mode. In this mode, the X-ray pulse starts from electron shot noise [5]. The temporal and spectral coherences of X-ray SASE pulses is poor. Various self-seeding schemes that employ gratings and Bragg crystals can mitigate this problem [6–10]. To further improve longitudinal coherence and reduce fluctuations, seeding with an external laser has been successfully implemented for wavelengths larger than a few nanometers [11]. In hard X-rays range, several cavity-based schemes are being implemented [12, 13]. An alternative approach of creating coherent narrow bandwidth hard X-ray pulses is the X-ray Laser Oscillator [14]. In XLO, a train of SASE pump pulses with spacing τ periodically strikes a liquid jet creating a population inversion. The resulting ASE radiation is recirculated in a Bragg cavity for further amplification rounds, before it is outcoupled. Rapid gain medium delivery is crucial for XLO operation, as it needs to be completely refreshed before the next pumping pulse arrives. In the original XLO proposal, subsonic jets of up to 250 m/s were considered.

XLO is currently under construction at SLAC National Laboratory. The gain medium chosen for this first experiment is a solution of cupric nitrate. Here we report on the gain medium delivery optimization, using the open-source CFD code OPENFOAM and the radiation hydro-code FLASH. We will also consider solid targets. For Fig. 1 please refer to [14] for the detailed XLO concept description.
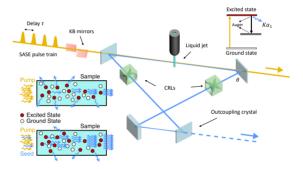

Figure 1: XLO schematics.

JET NOZZLE DESIGN AND FLUID PARAMETERS

For the first round of XLO experiments, we initially considered three different nozzles of 210 μm, 160 μm and 100 μm, respectively. The key problem is providing the liquid jet through the nozzle that has a) high velocity b) optically homogeneous, with minimal disturbances on its surface. The nozzles were made from mm glass tubes, by hot-rolling to a specified diameter. The nozzle was positioned close to the cone-shaped catcher, providing just enough clearance for the XFEL pulse; see Fig. 2. We have measured the density and viscosity of the copper nitrate solution in 3, 4 and 5 molar concentrations. The results were 4.05 mPa s for 3 molar, 8.0 mPa s for 4 molar and 16 mPa s for 5 molar solutions. We note that our jet is very different from previously studied water micro-jets, e.g. in [15–17]. The jet was placed in a sealed Helium chamber. We have developed speeds of up to 100 m/s in the first tests. In practical terms, we are handicapped by the volume flux and pressure drop attainable by the pump currently at our disposal.
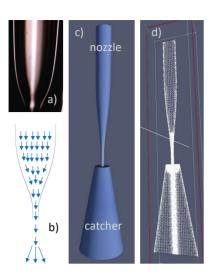
Figure 2: XLO jet nozzle design: a) microscopic image of the glass nozzle b) schematics of the gain medium flow in the nozzle c) reconstructed 3D model and d) mesh diagram of the nozzle and catcher setup.

NUMERICAL SIMULATIONS OF THE LIQUID JET

We have built a numerical model of liquid ejection from nozzle and traveling through He media. We used the finite volume two-phase (VOF) solver interFoam from OPEN-FOAM framework and generated a hexagonal adaptive mesh with boundary layers near nozzle surface. First, the nozzle model, such as depicted in Fig. 2 c) is analyzed with the OPENFOAM BLOCKMESH and SNAPPYHEXMESH utilities to generate a mesh for the finite volume solver. The initial and boundary conditions for the velocity (U), pressure (P), temperature (T), and turbulence variables are defined over the entire 3D simulation domain. It is important to choose an appropriate amount of grid cells, as the model may become divergent in the narrowest part of the nozzle. The simulation domain was refined by optimizing the Courant number, in order to ensure the stability of the numerical method. The nozzle geometry impacts the jet velocity and divergence. At subsonic speeds it is expected for the jet to exhibit turbulence. We modelled these effects using the time-dependent or Reynolds-averaged Navier-Stokes (RANS) model. Our simulations show that the wettability and adhesion in the nozzle play a crucial role in the fast cupric nitrate jet formation. For instance, for the smallest nozzle of 100 μm we observe a very high jet velocity drop 2 mm away from the nozzle. Figure 3 shows that for every nozzle diameter a stationary jet is formed. Velocity distribution in jet is relaxing from a typical parabolic-like profile in the nozzle to a uniform, after some distance, with the narrower the nozzle, the faster. This occurs due to the jet-surface contact layer being much slower than the rest of the jet, albeit comparable in thickness

with the fast core part. We also observe spray formation (experimentally), effectively reducing the jet transverse density. We conclude that although one can reach very high speeds with the small aperture nozzle and high pressure pump, its dynamics is very complicated and it makes these nozzles quite impractical for fast speed jets.

On the contrary, with a larger 200 μm nozzle the jet velocity becomes flow-rate limited, requiring very high mass flow-rates (liters per minute) to reach high speeds; see Figs. 3 and 4. These flow rates are currently not available in precise scientific grade pumps, thus an industrial precision pump should be used. Larger nozzle diameter makes the jet velocity much more controllable, allowing for a longer travel distance before developing spray layer. We therefore used 160 μm and 200 μm in the jet experiments. We note that for laminar low speed jets the aforementioned effects are not strong and the nozzle diameter can be selected according to the sample requirements.
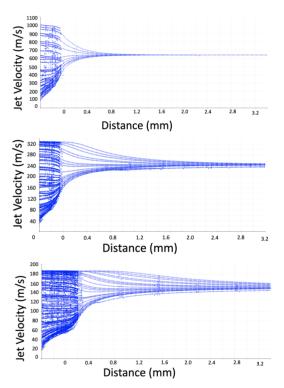

Figure 3: OPENFOAM simulations of jet velocity distribution in case of 100 μm (top), 160 μm (middle) and 200 μm (bottom) nozzles as a function of distance from the nozzle exit.

Figure 4: Current distribution of the jet in case 200 μm nozzle.

NUMERICAL SIMULATIONS OF THE XFEL-JET INTERACTION

The expansion of the plasma channel, formed after the initial ionization was simulated using FLASH (adaptive mesh hydrodynamic code solver) [18]. It supports an equation of state and opacity based multi-temperature treatment of the plasma. Since the photoionization and Auger decay are expected to be the dominant processes, the temperature of the electrons initially is significantly different from the ions. The ions and electrons would gain energy from the high energy electrons and would subsequently thermalize. This thermalization rate can be estimated using Spitzer conductivities. The electron-electron equilibration happens at a much shorter timescale (about 0.01 ps) than the electron-ion equilibration (about 100 ps) in the initial distribution of the ions was assumed to be negligible even after the XFEL pulse leaves the medium. This ionization level could be calculated assuming an energy deposition of the entire pulse over the width of the XFEL pulse and the attenuated length. By considering the dominant processes, the ionization level was assumed to be 2 and the corresponding upper limit for the electron temperature after thermalization was estimated to be around 1 keV, while the ions were assumed to be at the room temperature. The expansion of the plasma column was modelled using a 3D Cartesian geometry and a Cartesian mesh consisting of $(8)^3$ blocks is used to resolve a $(200\,\mu m)^3$ long simulation window with a maximum refinement level of 2. The liquid jet has a diameter of 160 μm and the plasma column having radius of has an initial radius of 1 μm. The electron temperature of the plasma column was set at 1 keV at the edge of the jet and it was exponentially decayed with an attenuated length of 81.36 μm. The size of the gap at time, t = 10 ns after initialization and the simulation window is shown in Fig. 5.
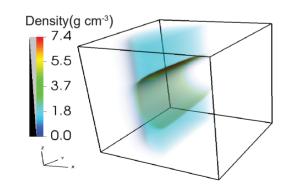

Figure 5: FLASH simulation snapshot showing the size of the gap at time, t = 10 ns after the XFEL-induced volume excitation.

SOLID TARGET GAIN MEDIUM

Solid targets are also being consider as gain media for the XLO. Such a target has several advantages over a liquid-based target including much higher densities of the target atom (several orders of magnitude), higher overall density reducing x-ray induced explosion effects, and having no other atomic species to interact with either the pump or emitted x-rays. However, unlike a liquid jet, solid targets are not intrinsically self-healing and must be treated as a finite resource. This, coupled with the need to very quickly replace the gain medium between pulses, makes the use of solid targets challenging. Several options capable of achieving the requisite medium velocity have been considered including magnetically levitated and rotated targets [19], capable of achieving tip speeds in excess of 1000 m/s, and ultra-fast MEMS movers [20]. For initial tests though, commercial off-the-shelf (COTS) brushless motors and controllers will be used. Readily available motors are able to spin a solid target disk with tip velocities well over the 100 m/s needed for initial testing. By controlling the rotation speed relative to the x-ray pulse frequency, efficient use of the finite target material can be made, especially by moving the rotating target laterally at relatively slow speeds: only a few microns, dependent on the size of the region affected by the x-ray induced explosion, of lateral motion per revolution would refresh the medium in time for the next X-ray pulse.

Preliminary tests of this concept using COTS hardware are underway to characterize the stability and controllability of the rotational speed of a copper disk target. Subsequent testing will use optical lasers to simulate the x-ray ablation to check the mechanical stability of the target when subject to perturbations. Finally, future x-ray interaction tests are planned which will serve as a proof-of-concept for solid state XLO gain media. An added benefit of this scheme is that, by adjusting the angle between the disk normal and the x-ray beam, the length of the interaction region can be freely controlled, allowing for experimental optimization.

SUMMARY

We utilized INTERFOAM solver to propagate liquid solution of cupric nitrate in helium atmosphere. Our CFD simulations indicate that a 200 μm diameter jet provides stable, well-collimated flow, while its velocity is being limited by the flow-rate of the pump. On the contrary, a 100 μm jet is much faster, but its velocity profile and current profile rapidly degrade after exiting the nozzle. We are also investigating fast moving solid targets as XLO gain medium. We note that development of rapid sample delivery is not only important for XLO but also for the future high-repetition rate XFELs.

ACKNOWLEDGEMENTS

REFERENCES

[1] N. Rohringer *et al.*, "Atomic inner-shell X-ray laser at 1.46 nanometres pumped by an X-ray free-electron laser", *Nature*, vol. 481, p. 488, Jan. 2012. `doi:10.1038/nature10721`

[2] H. Yoneda *et al.*, "Atomic inner-shell laser at 1.5-ångström wavelength pumped by an X-ray free-electron laser", *Nature*, vol. 524, pp. 446-449, Aug. 2015. `doi:10.1038/nature14894`

[3] T. Kroll *et al.*, "Stimulated X-Ray Emission Spectroscopy in Transition Metal Complexes", *Phys. Rev. Lett.*, vol. 120, p. 133203, Mar. 2018. `doi:10.1103/PhysRevLett.120.133203`

[4] T. Kroll *et al.*, "Observation of Seeded Mn $K\beta$ Stimulated X-Ray Emission Using Two-Color X-Ray Free-Electron Laser Pulses", *Phys. Rev. Lett.*, vol. 125, p. 037404, Jul. 2020. `doi:10.1103/PhysRevLett.125.037404`

[5] R. Bonifacio *et al.*, "Collective instabilities and high-gain regime free electron laser", *AIP Conference Proceedings*, vol. 1, pp. 236-2593, Jul. 1984. `doi:10.1063/1.34640`

[6] D. Ratner *et al.*, "Experimental Demonstration of a Soft X-Ray Self-Seeded Free-Electron Laser", *Phys. Rev. Lett.*, vol. 114, p. 054801, Feb. 2015. `doi:10.1103/PhysRevLett.114.054801`

[7] J. Amann *et al.*, "Demonstration of self-seeding in a hard-X-ray free-electron laser", *Nature Photonics*, vol. 6, pp. 693-698, Oct. 2012. `doi:10.1038/nphoton.2012.180`

[8] I. Inoue *et al.*, "Generation of narrow-band X-ray free-electron laser via reflection self-seeding", *Nature Photonics*, vol. 13, p. 1, May 2019. `doi:10.1038/s41566-019-0365-y`

[9] T. Osaka *et al.*, "A micro channel-cut crystal X-ray monochromator for a self-seeded hard X-ray free-electron laser", *Journal of Synchrotron Radiation*, vol. 26, pp. 1496–1502, Sep. 2019. `doi:10.1107/S1600577519008841`

[10] I. Nam *et al.*, "High-brightness self-seeded X-ray free-electron laser covering the 3.5 keV to 14.6 keV range", *Nature Photonics*, vol. 15, pp. 435-441, Mar. 2021. `doi:10.1038/s41566-021-00777-z`

[11] O. Yu. Gorobtsov *et al.*, "Seeded X-ray free-electron laser generating radiation with laser statistical properties", *Nature Communications*, vol. 9, p. 4498, Oct. 2018. `doi:10.1038/s41467-018-06743-8`

[12] K. Kim *et al.*, "A Proposal for an X-Ray Free-Electron Laser Oscillator with an Energy-Recovery Linac", *Phys. Rev. Lett.*, vol. 100, p. 244802, Jun. 2008. `doi:10.1103/PhysRevLett.100.244802`

[13] G. Marcus *et al.*, "Refractive Guide Switching a Regenerative Amplifier Free-Electron Laser for High Peak and Average Power Hard X Rays", *Phys. Rev. Lett.*, vol. 125, p. 254801, Dec. 2020. `doi:10.1103/PhysRevLett.125.254801`

[14] A. Halavanau *et al.*, "Population inversion X-ray laser oscillator", *National Academy of Sciences*, vol. 117, pp. 15511–15516, Jul. 2020. `doi:10.1073/pnas.2005360117`

[15] C. A. Stan *et al.*, "Liquid explosions induced by X-ray laser pulses", *Nature Physics*, vol. 12, pp. 966-971, Oct. 2016. `doi:110.1038/nphys3779`

[16] U. Weierstall *et al.*, "Lipidic cubic phase injector facilitates membrane protein serial femtosecond crystallography", *Nature Communications*, vol. 5, p. 3309, Feb. 2014. `doi:10.1038/ncomms4309`

[17] M. O. Wiedorn *et al.*, "Rapid sample delivery for megahertz serial crystallography at X-ray FELs", *IUCrJ*, vol. 5, pp. 574–584, Sep. 2019. `doi:10.1107/S2052252518008369`

[18] B. Fryxell *et al.*, "FLASH: An Adaptive Mesh Hydrodynamics Code for Modeling Astrophysical Thermonuclear Flashes", *The Astrophysical Journal Supplement Series*, vol. 131, pp. 273–334, Nov. 2000. `doi:10.1086/317361`

[19] M. Schuck *et al.*, "Ultrafast rotation of magnetically levitated macroscopic steel spheres", *Science advances*, vol. 4, p. e1701519, Jan. 2018. `doi:10.1126/sciadv.1701519`

[20] D. Mukhopadhyay *et al.*, "X-ray photonic microsystems for the manipulation of synchrotron light", *Nature Communications*, vol. 6, p. 7057, May 2015. `doi:10.1038/ncomms8057`